Microcellular approach to submandibular gland senescence. Myoepithelial markers between aging and tumors

Shereen AbdelFattah, Hossam Yehia, Tarek AbdelGalil

Anatomy and Embryology, Kasralainy, Faculty of Medicine, Cairo University, Cairo, Egypt

SUMMARY

Advance in age outcomes changes that disrupts the function of the salivary glands which are weakened vigorously. Advanced worsening in the histological structure of submandibular gland alters production of saliva. This study was hypothesized to point out the micro-cellular variations with aging in submandibular salivary glands, moreover to detect the role of myoepithelial markers and the propensity of malignant transformation with aging. Fifty male rats were used: group I (young adult), group II (senile). Light microscopic techniques (H&E, Masson trichrome, immunohistochemistry for vimentin, cytokeratin and PCNA) and electron microscopy were used. MDA, GSH and SOD, and a molecular study for p53 was evaluated.

The submandibular gland of old rats shows variable sized, shrunken acini, and necrosis. Swollen intercalated ducts with eccentric lumina, and irregular striated ducts are reported. E.M. revealed degenerated myoepithelial cells, cytoplasmic rarefaction, marked reduction of the nuclear chromatin, large macrophages with large lysosomes and many endocytic vesicles. The mean area percent of collagen fibers, vimentin, and cytokeratin in senile rats exposed significant increase and a significant decrease of mean number of PCNA cells when compared to young rats. The mean values of MDA, P53 revealed a significant surge, while that of GSH and SOD exhibited a significant decline when compared to adult rats. Vimentin and cytokeratin have a direct correlation with aging in the submandibular gland. They are concomitant with hyperplastic changes in the gland so they might be a strong indicator of presence of a tumor.

Key words: Submandibular gland – Aging – Vimentin – Cytokeratin – Tumor markers

INTRODUCTION

Aging causes physiological changes that disrupt the function of all tissues (Lopez-Otin et al., 2023), as well as significant damage to the salivary glands. Numerous investigations have demonstrated gradual deterioration in the architecture of salivary glands, as well as changes in saliva capacity with age. Age-related salivary changes are mostly induced by acinar cells; as a result, decreased saliva levels have unsettling consequences, includ-

Corresponding author:
Shereen Abdelfattah. Dept. of Anatomy and Embryology, Kasralainy, Faculty of Medicine, Cairo University, Cairo 11562, Egypt. Phone: 01099060936; Fax: 0235875958. E-mail: dr_shery.fattah@yahoo.com

Submitted: November 29, 2023. **Accepted:** May 2, 2024

https://doi.org/10.52083/NDHQ3891

ing vulnerability to alveolar caries, infections, and deglutition issues, all of which impair life quality (Toan and Ahn, 2021; Smith et al., 2013). Multiple variables contribute to salivary gland aging. Unfortunately, there is no absolute cure to repair the irreversible damage to the salivary glands. Therefore, examining the corresponding underlying etiology and molecular biology affecting salivary gland efficiency throughout aging is beneficial (Li et al., 2013).

Reactive oxygen species (ROS) liberation was exhibited to cause oxidative insult to oral proteins, lipids, and DNA, leading in cellular damage (Zalewska, 2016).

There are multiple epithelial tumors in salivary glands, which can be benign or malignant, according to the sorting of the World Health Organization. These tumors reveal diversity in histology and features. While diagnosis can be done with hematoxylin-eosin, immunohistochemistry constutes an important tool to categorize the cellular differentiation and allocate precise organizations in several cases (Zhu et al., 2015). Myoepithelial carcinoma is a tumor in the salivary glands, in which cancer cells display exclusively myoepithelial differentiation. Immune-expression for keratins and a myoepithelial marker is compulsory to identify myoepithelial tumors. Myoepithelial tumors commonly prompt vimentin and cytokeratins (Barnes, 2005; Saveral et al., 2005). Vimentin is an indicator of epithelial–mesenchymal transition EMT (Adams et al., 2015). Raised vimentin levels have been distinguished in several cancers, such as prostate cancer (Satelli, 2011) and esophageal carcinoma (Irani et al., 2014).

Apoptosis is a dynamic process, in which cell reduction, chromatin condensation and DNA fragmentation are indorsed. Cancers often derestrict apoptosis in, being this technique an appropriate goal as anticancer agent (Cotter, 2009). p53 normally is a tumor suppressor gene. Mutation of p53 is amongst the most frequently perceived gene abnormalities in neoplasia (Tarakji et al., 2012). The damage of function of p53 might result in the progress of various types of cancer.

Furthermore, the presence of genes involved in cell proliferation and oncogenesis appears to be correlated with the prognosis of oral cancers. Proliferating cell nuclear antigen (PCNA) determines the course of cellular proliferation, and thus the susceptibility to malignant conversion (Alves, 2002). Tumor development is dependent on its angiogenic activity. Blood vessels are newly produced and necessary for the development of the tumor (Tadbir et al., 2012).

This study was carried out in order to study the microcellular alterations with aging in submandibular salivary glands, as well as the role of myoepithelial markers and the tendency of malignant transformation with aging; moreover, the role of p53 and PCNA in the senescence process were illustrated.

MATERIALS AND METHODS

Animals

Fifty adult Wistar male rats, their weights range being from 150 to270 g, were used. The male rats were used in order to avoid any possible hormonal effects on the experiment.

The rats were obtained from the House of Animals, Faculty of Medicine, Cairo University. The study followed the guidelines of the Committee of Ethics of the Faculty of Medicine of Cairo University and the University of New Giza. All procedures observed the controlling principles for experimental rats. The work was carried out in accordance with the ethical guidelines of the Institutes of National Health's directory for the care of Laboratory Animals (NIH Publications No. 8023, revised 1978). The rats underwent a two-week period of adaptation in the laboratory before carrying out the experiment. They were kept in cages, five rats per cage, under standard laboratory and environmental conditions and were given standard rodent food and water *ad libitum.*

Experimental Design: 50 rats were used in this study, divided into 2 groups: Group I (25 rats): young adult rats (age ranged from 4-6 months); Group II (25 rats): senile rats (age ranged from 22-24 months). The rats of each group were sacrificed with an overdose of intraperitoneal phenobarbital sodium (40 mg/kg).

Ultrastructural preparations

For electron microscope, parts of the submandibular gland from each rat were fixed in 2% paraformaldehyde and 2% glutaraldehyde solution in 0.1 mol/L phosphate buffered saline (PBS) pH 7.2, and reserved in the refrigerator overnight, rinsed in 0.1 mol/L PBS and postfixed in phosphate-buffered 1% osmium tetroxide. To acquire cross-sections, the gland samples were oriented longitudinally in a flat mold and then embedded in resin. Semithin cross-sections were stained with 1% toluidine blue, and then examined by light microscope for proper orientation and image analysis of axons number. Ultrathin sections (50-60 nm) were stained with uranyl acetate and lead citrate. These sections were examined and photographed using a Jeom-1400 transmission electron microscope (JEOL Ltd./Japan a Joel), Electron Microscopy Department, Faculty of Agriculture, Cairo University, Egypt.

Light microscopic study

The submandibular gland of each rat was expunged and organized for paraffin blocks, 5 µm thick, which were obtained using a microtome then mounted on glass slides (Bancroft and Gamble, 2008). The slides were used for both histological and immunohistochemical study.

- Hematoxylin and eosin stain
- Masson's trichrome stain
- Immunohistochemistry

Paraffin sections were dewaxed, rehydrated and incubated with 3% hydrogen peroxide solution for half an hour at room temperature (RT) and endogenous peroxidase activity was blocked by treatment with 0.9% hydrogen peroxide in absolute methanol for 10 min. Then, the sections were washed with distilled water; a microwave was utilized for tissue antigen retrieval with sodium citrate buffer solution (pH = 6). Afterwards, slices were splashed with distilled water, and put into phosphate-buffered saline (PBS) for 5 min. After PBS was rubbed off, 5% normal goat serum was added onto the section at RT for 30 min. Deparaffinized sections of the submandibular gland were incubated for 30 min at RT with vimentin mouse monoclonal antibody (V9) (#:MA5-11883 dilution 1:100), anti-pan cytokeratin (anti-CK AE1/AE3) (#:MA5-13156 dilution 1:100) and anti-PCNA, which is a mouse monoclonal antibody ([PC10] antibody ab29, 1:200). Antibodies were obtained from Thermo Fisher Scientific Industries (Waltham, MA, USA). Slides were bathed well in PBS (3 times, 2 minutes each), incubated for 20 minutes with 2 drops of biotinylated secondary antibody for each section, and then rinsed well with PBS. Substrate chromogen (DAB) mixture 2 drops were applied for 5 minutes then rinsed well with distilled water. Slides were counterstained with hematoxylin, dehydrated and mounted. Negative controls were accomplished with a method similar to the one declared, except that the primary antibody was exchanged by non-immune serum.

Histomorphometric study

Quantitative data were attained using Leica Qwin 500 Image Analyzer software system (National Institute of Mental Health, Bethesda, Maryland, USA). The slides were examined within the standard measuring frame of a known area equal to 11694 μm^2. The removal of quantitative information from images was the final stage of analysis. The following parameters were examined at X40 objective lens in 10 non-overlapping fields for each gland in all animal groups:

i. Area percentage of collagen fibers in Masson's trichrome-stained sections.

ii. Area percentage of vimentin, cytokeratin and the cell count of PCNA.

Biochemical assays

Tissue levels of oxidative/ antioxidative markers

- **Oxidative stress markers (MDA):**

The submandibular MDA was measured according to the manufacturer's instructions. The resources for this method were delivered as kits by (Biodiagnostics, Cairo, Egypt).20 mg of tissue was homogenized in 1 mL PBS, pH 7.0 with a micro pestle in a micro tube. 20% TCA was added to tissue homogenate to precipitate the protein and centrifuged. Supernatants were collected and thiobarbituric acid (TBA) solution was added to the supernatants. After boiling for 10 minutes in water bath, the absorbance was measured. The

concentration of MDA was calculated using the standard curve.

- **Anti-oxidative stress markers:**

The SOD (Biodiagnostics, Cairo, Egypt) activity in tissue homogenate was premeditated by the clampdown of nitroblue tetrazolium drop via the generated O2 by the oxidase system (xanthine/ xanthine). Single SOD action unit was demarcated as the amount of enzyme instigating 50% embarrassment in 1 ml reaction solution per milligram tissue protein. The procedures were prepared affording the manufacturer's information. GSH (Biodiagnostics, Cairo, Egypt) calculations are built on the discount of 5, 5 dithiobis (2-nitrobenzoic acid) (DTNB) with condensed glutathione to yield a yellow composite. The condensed chromogen is straightly proportionate to GSH application (absorbance is measured at 405 nm).

Real time Quantitative PCR P53, VEGF

The qualified abundance of mRNA species was evaluated using theSYBR Green method on an ABI prism 7500 sequence detector system (Applied Biosystems, Foster City, CA). PCR primers were designed with Gene Runner Software (Hasting Software, Inc., Hasting, NY) from RNA sequences from Gen Bank.All primer sets had a calculated annealing temperature of 60°C. Quantitative RT-PCR was performed in a 25 µl reaction volume consisting of 2X SYBR Green PCR. Gene primers sequences were as follows:

P53:

Forward primer: (5-ATGTTTTGCCAACTGGCCAAG-3)

Reverse primer: (5-TGAGCAGCGCTCATGGTG-3)

Beta-Actin:

Forward primer: (5-ATC TGG CAC CAC ACC TTC-3)

Reverse primer: (5-AGC CAG GTC CAG ACG CA-3)

Master Mix (Applied Biosystems), 900 nM of separate primer and 2-3 µl of cDNA. Augmentation conditions were 2 min at 50°C, 10 min at 95°C and 40 cycles of denaturation for 15s and annealing/extension at 60°C for 10 min. Data from real-time assays were measured using the v1•7 Sequence Detection Software from PE Biosystems (Foster City, CA).Relative countenance of studied gene mRNA was designed using the comparative Ct method. All values were normalized to the beta actin gene and reported as fold change**.**

Statistical analysis

Statistical analysis was performed using statistical package for social sciences (SPSS) version 21.0 (IBM Corporation, Somers, NY, USA) statistical software. The results were expressed as means ± standard deviation (SD). Statistical evaluation was done using independent T test. Significance was considered when p value is ≤ 0.05 throughout the study.

RESULTS

Histological study on age-related changes in submandibular glands

H & E-stained sections

The submandibular gland of young rats is taken at the junction of the serous and mucous parts of the gland. There are large numbers of serous acini and mucous acini which are apparently healthy, intercalated ducts, and striated ducts. The field shows a large number of apparently healthy mucous acini. The acinar cells are pyramidal in shape, with vacuolated cytoplasm and peripheral flattened nuclei. Some acini are capped with serous demilunes, myoepithelial cells and intercalated ducts, striated ducts with vesicular nuclei and clear basal striations are observed (Fig. 1a, b). The submandibular gland of old rats shows large number of serous acini that are variable in size and shape. Many acini are shrunken and some of their cells have lost their nuclei; the other cells show variable position of their nuclei. The intercalated ducts show swelling of the lining epithelium with eccentric lumina. Few striated ducts are healthy in appearance, while most of them are irregular in lining with disruption of their lining epithelium. The vessels in the vicinity of the main ducts are dilated and congested. The main ducts show hyperplasia of the lining epithelium. The striated duct shows cytoplasmic vacuolation with nuclear pyknosis. The arterioles show concentric hyper-

plasia of their media. The venules are dilated and congested, with swelling of the lining endothelial cells. There are areas of interstitial haemorrhage (Fig. 1c, d, e).

Ultrastructure (electron microscope)

Cross sections of the submandibular gland of a young rat show several mucus cells. Cells are healthy, with basal nuclei, rough endoplasmic reticulum and large number of mucus droplets. Blood vessels are noticed (Fig. 2a, b). Sections of the submandibular gland of senile rats, display some mucus cells. There are degenerated myoepithelial cells, with areas of cytoplasmic rarefaction. Most of the acinar cells are degenerated with marked reduction of the nuclear chromatin and

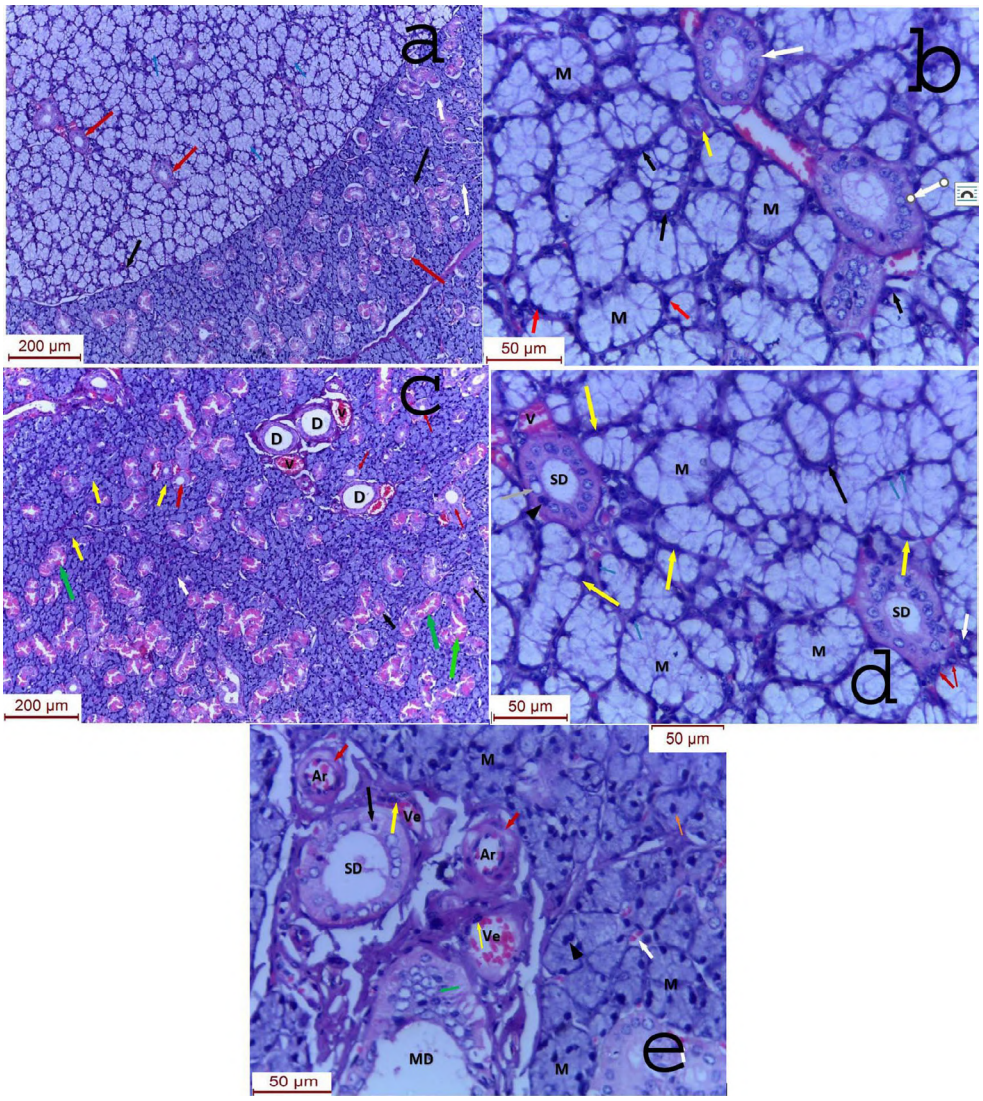

Fig. 1.- Cross sections of submandibular gland of a young rat. **a, b:** junction of the serous and mucous parts, serous acini (white arrows) and mucous acini (blue arrows) which are healthy. The black arrows indicate intercalated ducts, red arrows indicate striated ducts. There are healthy mucous acini, the acinar cells are pyramidal in shape, with vacuolated cytoplasm and peripheral flattened nuclei. Some acini are capped with serous demilunes (black arrows). The red arrows indicate myoepithelial cells. The yellow arrow indicates an intercalated duct, while the green arrows indicate striated ducts with vesicular nuclei and clear basal striations. Section of submandibular gland of an old rat. **c, d, e:** large number of variable sized serous acini (yellow arrows); shrunken acini and necrotic cells, and the other cells show variable position of their nuclei (white arrow). The intercalated ducts show swelling of the lining epithelium with eccentric lumina (black arrows). Few striated ducts are healthy (red arrows), while most of them are irregular with disruption of epithelium (green arrows). The vessels (V) in the vicinity of the main ducts (D) are dilated and congested. Most of the nuclei of the acinar cells are pyknotic (blue arrow). Most of the myoepithelial cells show pyknotic nuclei (yellow arrows). The intercalated ducts (white arrow) are reduced in size and its lining cells show pyknotic nuclei. The striated ducts (SD) are more or less healthy in appearance, with some of their lining cells are pyknotic (arrow head), and other cells show fatty degeneration (grey arrow). The serous demilunes (black arrow) are reduced in size, with disruption of their cells (red arrows). The vessels (V) in the vicinity of the striated ducts are dilated and congested. The main duct (MD) shows hyperplasia of the lining epithelium (green arrow). The striated duct (SD) shows cytoplasmic vacuolation with nuclear pyknosis (black arrow). The arterioles (Ar) show concentric hyperplasia of their media (red arrows). The venules (Ve) are dilated and congested, with swelling of the lining endothelial cells (yellow arrows). There are areas of interstitial haemorrhage (white arrows). (H&E). Scale bars: a, c = 200 µm; b, d, e = 50 µm.

marked cytoplasmic rarefaction. The rough endoplasmic reticulum is swollen and fragmented. There are macrophages with large lysosomes and many endocytic vesicles. The acinar basement membrane is thickened. Cells show marked cytoplasmic rarefaction with dispersion and fragmentation of the rER (Fig. 2c, d. e).

Masson trichrome stain

Masson's trichrome-stained sections of young rats showed slight amount of collagen fibers (Fig. 3a). Sections in old rats elucidated massive amount of collagen fibers around the ducts (Fig. 3b).

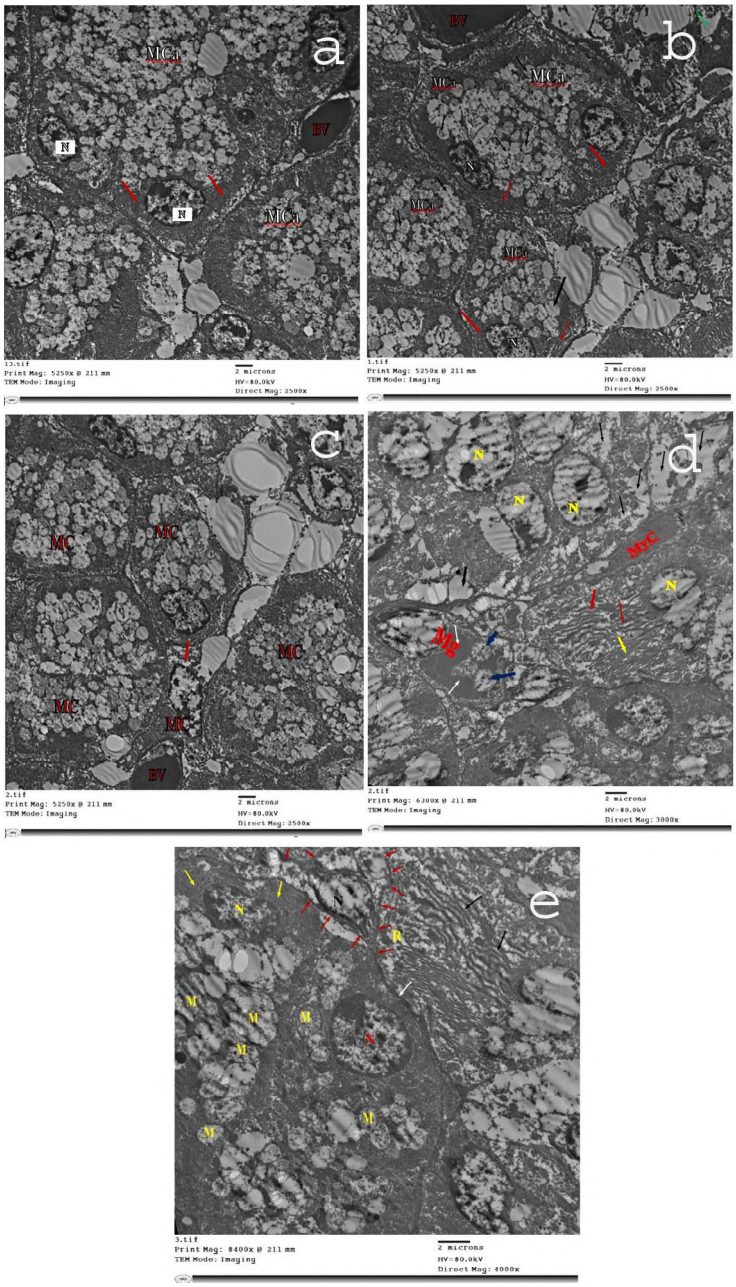

Fig. 2.- Electron micrographs of sections of the submandibular gland of a young rat (group I). **a, b:** several mucus cells. Healthy cells (MCa), basal nuclei (N), rough endoplasmic reticulum (red arrows) large number of mucus droplets (black arrows). BV refers to a blood vessel. Senile rats (group II) **c, d, e:** degenerated myoepithelial cell (MC), areas of cytoplasmic rarefaction (red arrow), blood vessel (BV), marked reduction of the nuclear chromatin (yellow N) and marked cytoplasmic rarefaction (black arrows), rough endoplasmic reticulum is intact in limited regions (yellow arrow), and is swollen and fragmented in other regions (red arrows), degenerated myoepithelial cell (MyC), macrophage (Mg) with large lysosomes (white arrows) and many endocytic vesicles (blue arrows). **e:** Section of the submandibular gland of an old rat, displaying the mucous portion of the gland. Some of the acinar cells are apparently normal, with basal flat nuclei (yellow N), parallel arrays of rough endoplasmic reticulum (yellow arrow) and large number of mucous droplets (M). Other cells show rounded nuclei (red N), with fewer areas of rER and mucous droplets. The acinar basement membrane is thickened (white arrow). Some cells show marked cytoplasmic rarefaction (R) with dispersion and fragmentation of the rER (black arrows). The red arrows delineate a necrotic myoepithelial cell with marked cytoplasmic rarefaction with a destroyed nucleus (black N). Scale bars: a-e = 2 µm.

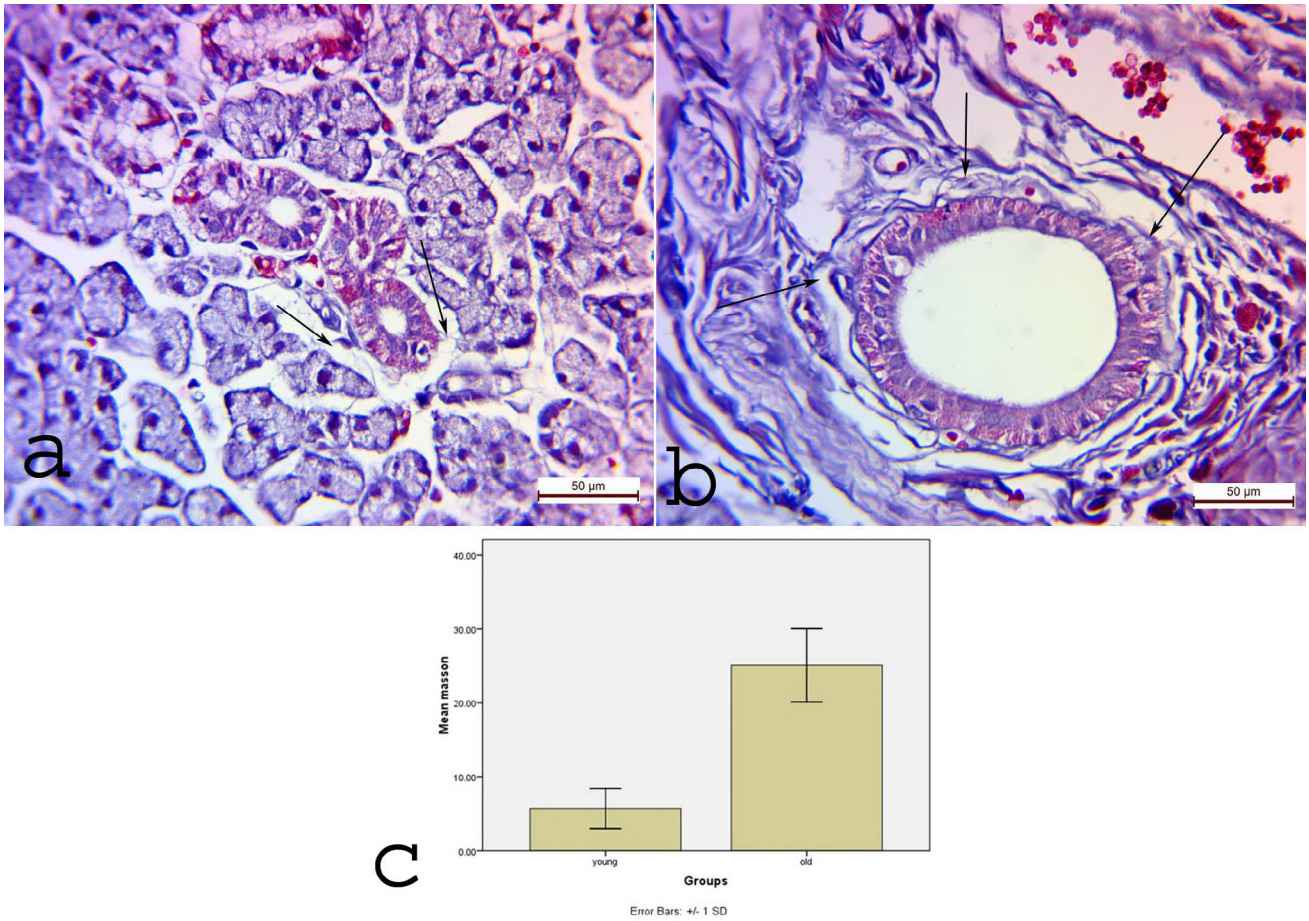

Fig. 3.- Sections of submandibular gland from group I. **a:** negligible amount of collagen fibers (arrows) around the duct (SD). Group II, **b:** immense amount of collagen fibers (arrows). Masson trichrome. Scale bars a-b = 50 µm.

Immunohistochemistry

Immune-expression; vimentin, cytokeratin young rats displayed weak positive immune-reaction and strong PCNA reaction in young rats (Fig. 4a, c, e). Sections of group old rats revealed strong positive immune-reaction around the acini of vimentin and cytokeratin and weak reaction of PCNA (Fig. 4b, d, f).

Histomorphometry

The mean area percent of collagen fibers, vimentin, and cytokeratin in senile rats revealed significant increment when compared to results of group I. Yet it showed a significant decrement of the mean number of PCNA cells (Tables 1 and 2).

Biochemical

MDA, SOD and GSH

The mean values of MDA in group II expressed a significant upsurge, while the mean values of SOD and GSH showed a significant reduction when compared to the values of group II (Table 3).

Real time PCR

P53

The mean values of P53 group II displayed significant raise when compared to the values of group II (Table 2).

Table 1. The mean area percent of collagen among the different groups.

	Group	Mean ± SD	Versus group	P value
Mean are % of collagen	young	5.68 ±2.71		
	Old	25.08 ±4.96	young	0 .004 *

* = Statistically significant

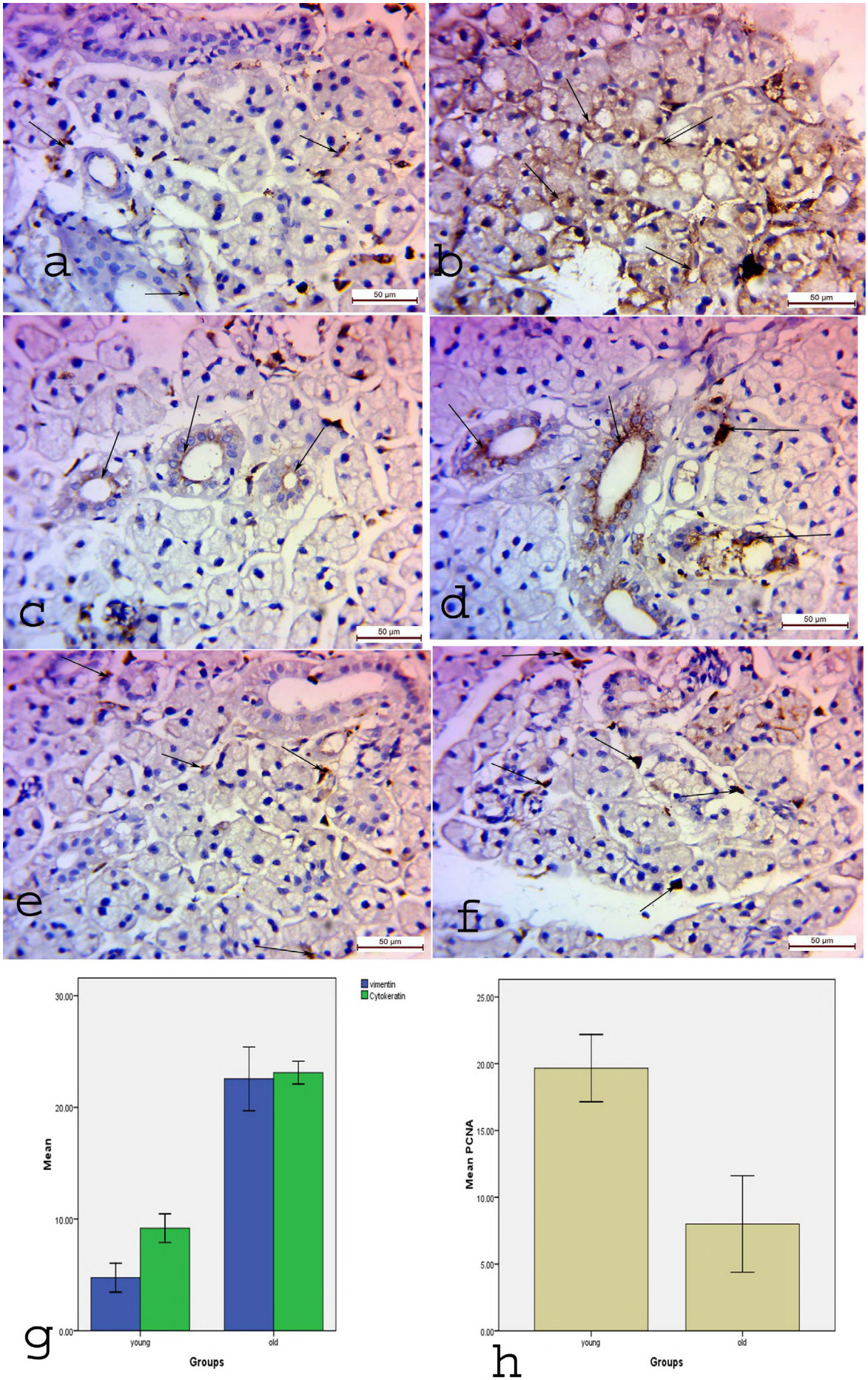

Fig. 4.- Sections of submandibular gland from group I. **a, c, e:** weak immunoexpression of vimentin, cytokertin and PCNA (arrows). Group II, **b, d, f:** strong immunoexpression of the previous parameters. Vimentin (a, b), Cytokertin (c, d) and PCNA (e, f). Scale bars = 50 µm.

Table 2. Comparison of cytokeratin, vimentin, P53 and PCNA among the different groups.

	Group	Mean ± SD	Versus group	P value
cytokeratin	Young	9.16±1.26		
	Old	23.11±1.018	young	0.000*
Vimentin	Young	4.75±1.29		
	Old	22.54± 2.85	young	0.001*
P53	Young	10.29±0.62		
	Old	31.84±7.59	young	0.008*
PCNA	Young	20 ±2.52		
	Old	8 ± 3.61	Young	0.01*
VEGF	Young	2.3 ± 1.1		
	Old	5.75±1.29	young	0.001*

* = Statistically significant

Table 3. Comparison of the oxidative markers among the different groups.

	Group	Mean ± SD	Versus group	P value
MDA	Young	5.45±3.28		
	Old	44.85±4.87	young	0.000*
GSH	Young	60.067±3.63		
	Old	27.56±6.017	young	0.001*
SOD	Young	5.07±1.71		
	Old	1.47±0.32	young	0.02*

* = Statistically significant

DISCUSSION

Many factors disrupt salivary glands as they age, causing compromise in their shape and function (Li et al., 2023). Senile rats' submandibular glands exhibited pathological changes, including variable-sized shrunken acini, necrotic cells, and a large intercalated disc with eccentric lumina. The veins in the area are dilated and clogged. The major ducts exhibit hyperplasia, cytoplasmic vacuolation, nuclear pyknosis, and increased collagen fiber content. The arterioles have concentric hyperplasia in their media. The venules are dilated and crowded, with enlargement of the endothelial cells that line them. There are places with interstitial hemorrhage. These findings agreed with Li et al. (2023), who attributed the structural change to a huge increase in connective tissue. This is verified with our results which illustrated a high significance when comparing the old group to the young ones

On the microcellular level we found degenerated myoepithelial cells, with areas of cytoplasmic rarefaction. Degenerated acinar cells with marked reduction of the nuclear chromatin and marked cytoplasmic rarefaction. The rough endoplasmic reticulum is swollen and fragmented. There are macrophages with large lysosomes and many endocytic vesicles. The acinar basement membrane is thickened. Cells show marked cytoplasmic rarefaction with dispersion and fragmentation of the rER. Li et al. (2023) propose an adverse correlation between autophagy and aging (Tai et al., 2017). The existence of traced constituents in lysosomes may be due to their decreased aptitude to wipe off intracellular contents (autophagy). The authors correlated the slow diminution of mitochondrial and autophagic actions with aging, which plays a critical part in the deterioration of glandular function (Green et al., 2011).

The mean values of MDA in group II exposed significant raise, while the mean values of SOD and GSH bare a significant reduction when compared to the values of group II. Oxidative stress has newly been a cause to interrupt cellular morphology, and this injurious procedure is a chief moderator in aging that ensues from disturbance of cell structure (Indo et al., 2015). ROS leads to stress and biological factors accumulate inside the body with the advance of age. Additionally, the interior anti-oxidative capability diminishes with age,and therefore the redox monitoring no longer works with full capacity (Dröge, 2003). This outcomes are oxidative strain and oxidative impairment.

Myoepithelial differentiation occurs in intermediate to senior age groups. One of its most prevalent sites is the submandibular gland (Vilar-González et al., 2015). Although myoepithelial tumors of the salivary gland are benign, they can progress to atypical malignancy if not treated properly (Weitzel et al., 2017).

Our results revealed that old rats displayed a strong positive immune-reaction of vimentin and cytokeratin around the acini, with a statistically significant surge compared to that of young rats. Similar results were reported by Zaki, et al.(2018). The authors reported that these transitional filaments were strongly exaggerated by oxidative stress. Zaki et al., (2018) instituted a positive correlation among amplified appearance of the myoskeletal filaments and MDA in the thyroid of senile groups. On the other hand, there is an adverse correlation between the countenance of intermediate filaments and antioxidative GSH and SOD, and these results were on the same line with our results, which documents the impact of the role of oxidative insult on the amplified expression of cytokeratin and vimentin.

Cytokeratin and vimentin intermediate filaments have like functions: they convey stress fight, part in signaling pathways, and backbone the cytoskeleton. Yet, their overexpression outcomes life-threatening variances in epithelial- and mesenchymal-like cells (Kuburich et al., 2024). Considering the properties of intermediate filaments in the cells that co-express of vimentin and cytokeratin as they might be a sign of cancer is critical for developing novel therapeutic options.

Group II displayed significant raise in p53 and decline in PCNA when compared to the values of group I. Senescence handicaps cellular proliferation, and it is well-thought-out as a process to defeat tumor-genesis (Campisi, 2001). However, senescence might trigger cells' robust apoptosis (Sasaki et al., 2001) and may permit mutations. Consequently, it has been claimed that senescence might protect creatures from cancers, but might induce cancers in elder life (Fossel, 2000; Sasaki t al., 2001).

Cao et al. (2003) assumed that senescence is most likely triggered by the stimulation of a p53-linked cell cycle that avoids cell proliferation. p53 activation is a key reason for the detected senescence. However, the genetic variability triggered can alter p53 and ultimately lead to tumorigenesis. The authors assumed that aging serves as a double-edged weapon that conquers tumorigenesis primary, but has lethal possessions far along.

We concluded that vimentin and cytokeratin have a direct correlation with aging in submandibular salivary gland. At the same time, they are concomitant with hyperplastic changes in the gland, so they might be a strong indicator of presence of tumor. Further studies are needed to investigate the correlation between the increment of expression of these filaments, senescence and tumorigenesis

REFERENCES

ADAMS A, WARNER K, PEARSON AT, ZHANG Z, KIM HS, MOCHIZUKI D, BASURA G, HELMAN J, MANTESSO A, CASTILHO RM, WICHA MS, NÖR JE (2015) ALDH/CD44 identifies uniquely tumorigenic cancer stem cells in salivary gland mucoepidermoid carcinomas. *Oncotarget*, 6(29): 26633.

ALVES FA, PEREZ DE, ALMEIDO OP, LOPES MA, KOWALSKI LP (2002) Pleomorphic adenoma of the submandibular gland: clinicopathological and immunohistochemical features of 60 cases of Brazil. *Arch Otolaryngol Head Neck Surg*, 128: 1400-1403.

BARNES L (ed.) (2005) *Pathology and genetics of head and neck tumour.* Vol. 9. IARC.

CAMPISI J (2001) Cellular senescence as a tumor-suppressor mechanism. *Trends Cell Biol*, 11(11): S27-S31.

CAO L, LI W, KIM S, BRODIE SG, DENG CX (2003) Senescence, aging, and malignant transformation mediated by p53 in mice lacking the Brca1 full-length isoform. *Genes Develop*, 17(2): 201-213.

COTTER TG (2009) Apoptosis and cancer: the genesis of a research field. *Nat Rev Cancer*, 9: 501-507.

DRÖGE W (2003) Oxidative stress and aging. *Adv Exp Med Biol*, 543: 191-200.

FOSSEL M (2000) Cell senescence in human aging: A review of the theory. *In Vivo*, 14: 29-34.

GREEN DR, GALLUZZI L, KROEMER G (2011) Mitochondria and the autophagy–inflammation–cell death axis in organismal aging. *Science*, 333(6046): 1109-1112.

INDO HP, YEN HC, NAKANISHI I, MATSUMOTO KI, TAMURA M, NAGANO Y, MATSUI H, GUSEV O, CORNETTE R, OKUDA T, MINAMIYAMA Y, ICHIKAWA H, SUENAGA S, OKI M, SATO T, OZAWA T, CLAIR DK, MAJIMA HJ (2015) A mitochondrial superoxide theory for oxidative stress diseases and aging. *J Clin Biochem Nutrit*, 56(1): 1-7.

IRANI S, SALAJEGHEH A, SMITH RA, LAM AK (2014) A review of the profile of endothelin axis in cancer and its management. *Crit Rev Oncol Hematol*, 89: 314-321.

KNAŚ M, MACIEJCZYK M, DANISZEWSKA I, KLIMIUK A, MATCZUK J, KOŁODZIEJ U, WASZKIEL D, ŁADNY JR, ŻENDZIAN-PIOTROWSKA M, ZALEWSKA A (2016) Oxidative damage to the salivary glands of rats with streptozotocin-induced diabetes-temporal study: oxidative stress and diabetic salivary glands. *J Diabetes Res*, 2016: 4583742.

KUBURICH NA, DEN HOLLANDER P, PIETZ JT, MANI SA (2022) Vimentin and cytokeratin: Good alone, bad together. In: *Seminars in cancer biology.* Vol. 86, pp 816-826. Academic Press.

LI N, YE Y, WU Y, LI L, HU J, LUO D, LI Y, YANG J, GAO Y, HAI W, XIE Y, JIANG L (2023) Alterations in histology of the aging salivary gland and correlation with the glandular inflammatory microenvironment. *iScience*, 26(5): 106571.

LOPEZ-OTIN C, BLASCO MA, PARTRIDGE L, SERRANO M, KROEMER G (2023) The hallmarks of aging: An expanding universe. *Cell*, 186(2): 243-278.

SASAKI M, KUMAZAKI T, TAKANO H, NISHIYAMA M, MITSUI Y (2001) Senescent cells are resistant to death despite low Bcl-2 level. *Mech Ageing Dev*, 122: 1695-1706.

SATELLI A, LI S (2011) Vimentin in cancer and its potential as a molecular target for cancer therapy. *Cell Mol Life Sci*, 68: 3033-3046.

SAVERA AT, SLOMAN A, HUVOS AG, KLIMSTRA DS (2000) Myoepithelial carcinoma of the salivary glands: a clinicopathologic study of 25 patients. *Am J Surg Pathol*, 24(6): 761-774.

SMITH CH, BOLAND B, DAUREEAWOO Y, DONALDSON E, SMALL K, TUOMAINEN J (2013) Effect of aging on stimulated salivary flow in adults. *J Am Geriatr Soc*, 61(5): 805-808.

TADBIR AA, PARDIS S, ASHKAVANDI ZJ, NAJVANI AD, ASHRAF MJ, TAHERI A, ZADEH MA, SARDARI Y (2012) Expression of Ki67 and CD105 as proliferation and angiogenesis markers in salivary gland tumors. *Asian Pac J Cancer Prev*, 13(10): 5155-5159.

TAI H, WANG Z, GONG H, HAN X, ZHOU J, WANG X, WEI X, DING Y, HUANG N, QIN J, ZHANG J, WANG S, GAO F, CHRZANOWSKA-LIGHTOWLERS ZM, XIANG R, XIAO H (2017) Autophagy impairment with lysosomal and mitochondrial dysfunction is an important characteristic of oxidative stress-induced senescence. *Autophagy*, 13(1): 99-113.

TARAKJI B, BAROUDI K, HANOUNCH S, NASSANI MZ, ALOTAIBI AM, KHARMA MY, AZZEGHAIBY SN (2012) Expression of P21 independent on or independent of P53 in carcinoma ex pleomorphic adenoma (undifferentiated and adenocarcinoma types). *Pol J Pathol*, 63(4): 286-291.

TOAN NK, AHN SG (2021) Aging-related metabolic dysfunction in the salivary gland: a review of the literature. *Int J Mol Sci*, 22(11): 5835.

VILAR-GONZÁLEZ S, BRADLEY K, RICO-PÉREZ J, VOGIATZIS P, GOLKA D, NIGAM A, SIVARAMALINGAM M, KAZMI S (2015) Salivary gland myoepithelial carcinoma. *Clin Transl Oncol*, 17(11): 847-855.

WEITZEL M, COHN JE, SPECTOR H (2017) Myoepithelioma of the parotid gland: a case report with review of the literature and classic histopathology. *Case Rep Otolaryngol*, 2017: 6036179.

ZAKI SM, MOHAMED EA, FATTAH SA, ABDULLAH H, KASZUBOWSKA L (2018) Age-associated functional morphology of thyroid and its impact on the expression of vimentin, cytokeratins and VEGF. The role of nigella in refinement. *Folia Histochem Cytobiol*, 56(3): 159-171.

ZHU S, SCHUERCH C, HUNT J (2015) Review and updates of immunohistochemistry in selected salivary gland and head and neck tumors. *Arch Pathol Lab Med*, 139(1): 55-66.